Research Paper

GEOSPHERE

GEOSPHERE; v. 12, no. 5

doi:10.1130/GES01321.1

10 figures; 4 tables

CORRESPONDENCE: jrjdavidson@gmail.com

CITATION: Davidson, J.R.J., Fairley, J., Nicol, A., Gravley, D., and Ring, U., 2016, The origin of radon anomalies along normal faults in an active rift and geothermal area: Geosphere, v. 12, no. 5, doi:10.1130/GES01321.1.

Received 27 January 2016
Revision received 22 June 2016
Accepted 9 August 2016

The origin of radon anomalies along normal faults in an active rift and geothermal area

Jonathan Robert Joseph Davidson[1], Jerry Fairley[2], Andrew Nicol[1,3], Darren Gravley[1], and Uwe Ring[1,4]

[1]Department of Geological Sciences, University of Canterbury, Private Bag 4800, Christchurch 8140, New Zealand
[2]Department of Geological Sciences, University of Idaho, 875 Perimeter Drive, MS 3022, Moscow, Idaho 83844, USA
[3]GNS Science, PO Box 30368, Lower Hutt, New Zealand
[4]Department of Geological Sciences, Stockholm University, Svante Arrhenius väg 8, SE-106 91 Stockholm, Sweden

ABSTRACT

Radon anomalies are widely reported in the vicinity of active faults, where they are often inferred to result from upward migration of fluids along fault zones. We examine the up-fault flow hypothesis by measuring radon (^{220}Rn and ^{222}Rn) in soil gas above two active normal fault zones within the central Taupo rift, New Zealand. In agreement with previous investigations, we find that the average concentrations of both radon isotopes are generally higher near mapped faults, although in some cases we find that the difference with background populations is not significant. Soil samples recovered from 1 m depth indicate that some of the radon anomalies along faults may reflect local changes in soil types. The ^{220}Rn isotope emanation measured from extracted soil samples shows a linear correlation with the field concentration measurements ($R^2 = 0.90$, p value = 3×10^{-6}), whereas ^{222}Rn emanation shows no linear correlation ($R^2 = 0.17$, p value = 0.17). The soil gas isotopes measured show a significant linear correlation of ^{220}Rn and ^{222}Rn concentrations ($R^2 = 0.44–0.55$, p value $<10^{-5}$) near faults. This correlation suggests a constant radon isotopic ratio is emitted from the soils tested, and this finding is supported by emission data measured on extracted soil samples. The distribution of ^{222}Rn concentration compared to ^{220}Rn can be explained by small-scale diffusion for >90% of the soil gas measurements, showing that a majority of radon anomalies along faults are not necessarily caused by advection of gases along fault planes and can be explained by an increase in radon soil emanation. However, diffusion cannot account for all of the observed patterns in the data, and in some specific locations along faults, ^{222}Rn concentrations are most likely produced by advective flow of subsurface gases, suggesting channelized gas flow in portions of some faults.

INTRODUCTION

Many investigations have reported radon anomalies at concentrations significantly higher than background levels along active faults (Tanner, 1978; Whitehead, 1984; King et al., 1996; Ciotoli et al., 1999; Al-Tamimi and Abumurad, 2001; Atallah et al., 2001; Ioannides, 2003; Burton et al., 2004; Font et al., 2008; Katsanou et al., 2010). The preponderance of evidence suggests that these anomalies can provide reliable information about the locations of faults and the spatial distribution of fluid flow within fault zones; however, the actual mechanism responsible for the observed radon anomalies is unclear. Local increases in radon emanation along faults could be caused by a number of processes, including coprecipitation of parent nuclides in groundwater mixing zones resulting in local fluctuations of radium decay in the soil (Tanner, 1964), increases in the surface area of faulted material by grain-size reduction (Holub and Brady, 1981; Tuccimei et al., 2010; Mollo et al., 2011; Koike et al., 2015), and carrier gas flow parallel to (and within) fault zones (e.g., King et al., 1996).

The consensus in recent publications is that the observed radon anomalies result from advective transport by carrier gases through high-permeability fault zones (King et al., 1996; Ioannides, 2003; Zarroca et al., 2012). In support of this hypothesis, it has been argued that faults are commonly associated with anomalous fluxes of a wide range of gases (CO_2, He, H_2) in addition to radon (King et al., 1996; Zarroca et al., 2012). For example, covariation between CO_2 gas flux and radon gas concentration proximal to faults suggests that in some cases CO_2 might be acting as a carrier gas (King et al., 1996). Investigators have also pointed out a lack of correlation between the concentration of radon parent isotopes radium (Ioannides, 2003) or uranium (King et al., 1996) and radon gas concentration in specific locations along the studied faults that they interpret as an indication of advective transport of radon-enriched gas, rather than as a reflection of changes in parent isotope concentration in the soils.

Given the acceptance that the concentrations of radon gas are the result of gas flow associated with elevated permeability in fault zones, radon soil gas surveys are widely regarded to be an effective tool to map buried or blind faults not detected during mapping of the surface geology (Whitehead, 1984; King et al., 1996; Al-Tamimi and Abumurad, 2001; Burton et al., 2004), and many studies do not consider other possible sources, such as the production of radon in near-surface soils (Whitehead, 1984; Al-Tamimi and Abumurad, 2001; Atallah et al., 2001; Katsanou et al., 2010). However, several lines of evidence from older publications suggest that fault-related anomalies could be produced by increased radium decay in soils (Tanner, 1978). For example, it has been suggested that local variations of soil composition may be responsible for differences in radon soil gas production as a result of the variability of

radioactivity in soils (Vogler, 1960), covariation between radon isotopes (Israel and Bjornsson, 1967), and/or the variability of the parent ^{226}Ra and daughter ^{222}Rn in soils (Tanner, 1964).

This paper focuses on understanding the processes that produce anomalies for two radon isotopes, ^{220}Rn and ^{222}Rn, proximal to active faults in the Taupo rift, New Zealand. To explore the possible mechanisms of radon transport near active faults, the concentration of ^{220}Rn and ^{222}Rn in soil gas was measured in the Maleme fault zone (MFZ) and along the Paeroa fault in the central Taupo rift (Fig. 1). Radon anomalies of each isotope were observed near faults in both field areas sampled. On the basis of our observations of the two radon isotopes at 1 m depth, we infer that radon anomalies in soil gas along the faults arise from both (1) increased radon soil emanation due to surface processes associated with faulting, and the resulting increased transport by diffusion, and (2) advective flow of gases along fault zones. In some areas of the Paeroa fault, localized increases of ^{222}Rn are more likely to be due to advective flow of gases and suggest channelized fluid flow within the fault zone, also marked by geothermal features, including hot springs and steaming ground. Although there is clear evidence for the occurrence of both processes, we find that in many locations along the faults surveyed, it is impossible to distinguish between the two. In such cases the assumption that fault-related anomalies are entirely due to advection may be incorrect.

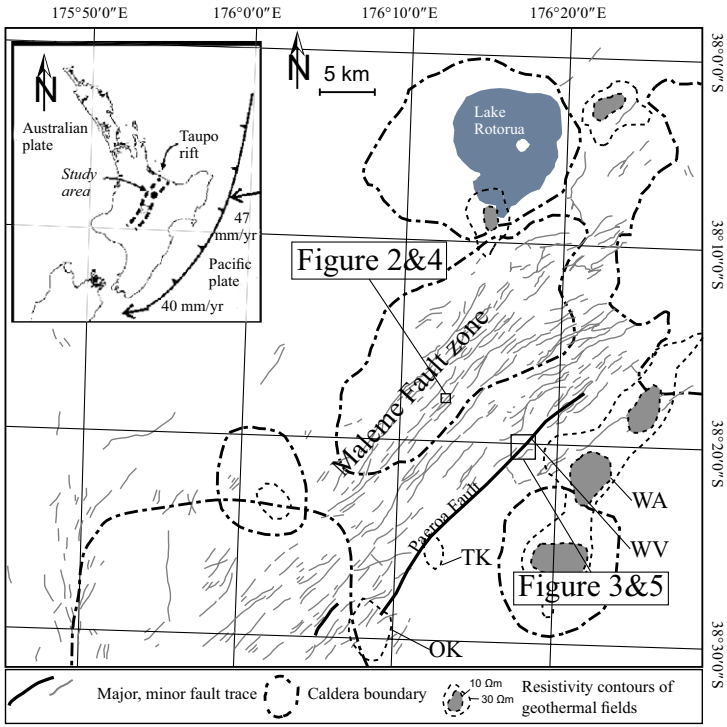

Figure 1. Map of the Ngakuru graben (modified from Bégué et al., 2014). Geothermally active areas: WV—Waikite Valley; TK—Te Kopia; OK—Orakei Korako, WA—Waiotapu.

GEOLOGICAL SETTING

Strong spatial relationships between radon anomalies and faults are recorded for active normal faults in the central Taupo rift (also referred to as the Taupo fault belt), a narrow zone (15–40 km wide) of active crustal extension spatially coincident with the central Taupo Volcanic Zone (TVZ). The TVZ is a 250-km-long northeast-trending area of mainly andesitic to rhyolitic arc-backarc volcanism within the continental crust of the central North Island, New Zealand (Cole, 1990; Wilson et al., 1995). Volcanism and rifting in the TVZ, which both formed in association with subduction of the Pacific plate during the past 1–2 m.y., produce crustal thinning and high average geothermal heat flow (~700 mW/m^2) (Wright, 1992; Bibby et al., 1995; Wilson et al., 1995; Rowland and Sibson, 2001; Stratford and Stern, 2006). Heat flow in the TVZ is highly variable, with zones of focused heat flow evidenced by the many geothermal fields, generally located in calderas and active volcanic centers. Within the part of the rift studied here, geothermal activity occurs at three locations along the Paeroa fault (Fig. 1).

For this study, radon anomalies along faults were observed in the Ngakuru Graben, a segment of the Taupo rift (Fig. 1). Radon soil gas surveys were conducted over two areas of active faulting (Fig. 1): (1) Rehi Road, which hosts multiple faults within the Maleme fault zone, and (2) Waikite Valley, where the Paeroa fault, the largest fault in the rift, is located. In both areas topographic scarps define fault locations, with Rehi Road having no geothermal activity, while Waikite Valley hosts numerous hot springs, fumaroles, and hydrothermal deposits. The two sites selected enabled radon concentrations to be measured for a range of fault sizes and geothermal conditions. At the Rehi Road site, for example, the scarps are significantly smaller (1–10 m high) than the 20–500 m scarps along the Paeroa fault at Waikite Valley. The precise location of the primary slip surface relative to the scarp is variable. At the Rehi Road site, slip surfaces are generally located at the bases of scarps; however, the exact location of the main slip surface along the Paeroa fault scarp is unclear, and could potentially be within the scarp. We refer to all topographic scarps associated with faulting simply as scarps.

In contrast to the geothermal activity that characterizes the Waikite Valley faults, normal faults at Rehi Road are not currently associated with hydrothermal activity and are located in a relatively cold part of the TVZ (Bibby et al., 1995). Rehi Road crosses the Taupo rift axis, which is defined by a series of scarps formed by normal faults known as the Maleme fault zone (MFZ; Fig. 1) (Villamor and Berryman, 2001; McClymont et al., 2009; Nicol et al., 2010). The MFZ has an overall trend of 055° and comprises as many as 16 discrete fault traces spaced at ~50–500 m that displace ca. 25 ka flat-lying fluviolacustrine sediments. Individual fault traces accommodate ~1–15 m maximum vertical

displacement of the ca. 25 ka surface, and the total vertical displacement rate in the MFZ is 1.85–3.55 mm/yr (Villamor and Berryman, 2001; Nicol et al., 2010). Trenches across active fault traces in the rift (including the Maleme fault zone) indicate that the faults cut a complex assemblage of tephra, paleosols, and alluvial deposits in the near surface (<6 m depth) (Villamor and Berryman, 2001; Berryman et al., 2008; Canora-Catalán et al., 2008; McClymont et al., 2009; Nicol et al., 2010). These fault zones typically comprise multiple slip surfaces, fault-bound lenses, fault splays, and local tectonic bed rotations (including smearing of clay-rich paleosols along faults) (e.g., Fig. 2). Direct observations from excavations suggest that the fault zones mainly range in width from 0.5 to 2 m, and that both the fault zone width and architecture can change dramatically over distances of 3–4 m. Fault zone width is usually significantly less than the scarp width (Fig. 2), with the deformation zone most often located in the lower half of the scarp (see trench logs in Villamor and Berryman, 2001; Berryman et al., 2008; Canora-Catalán et al., 2008; McClymont et al., 2009; Nicol et al., 2010).

The Waikite Valley area is located close to the northern end of the Paeroa fault, which hosts several hot springs and geothermal areas (Fig. 1). The Paeroa

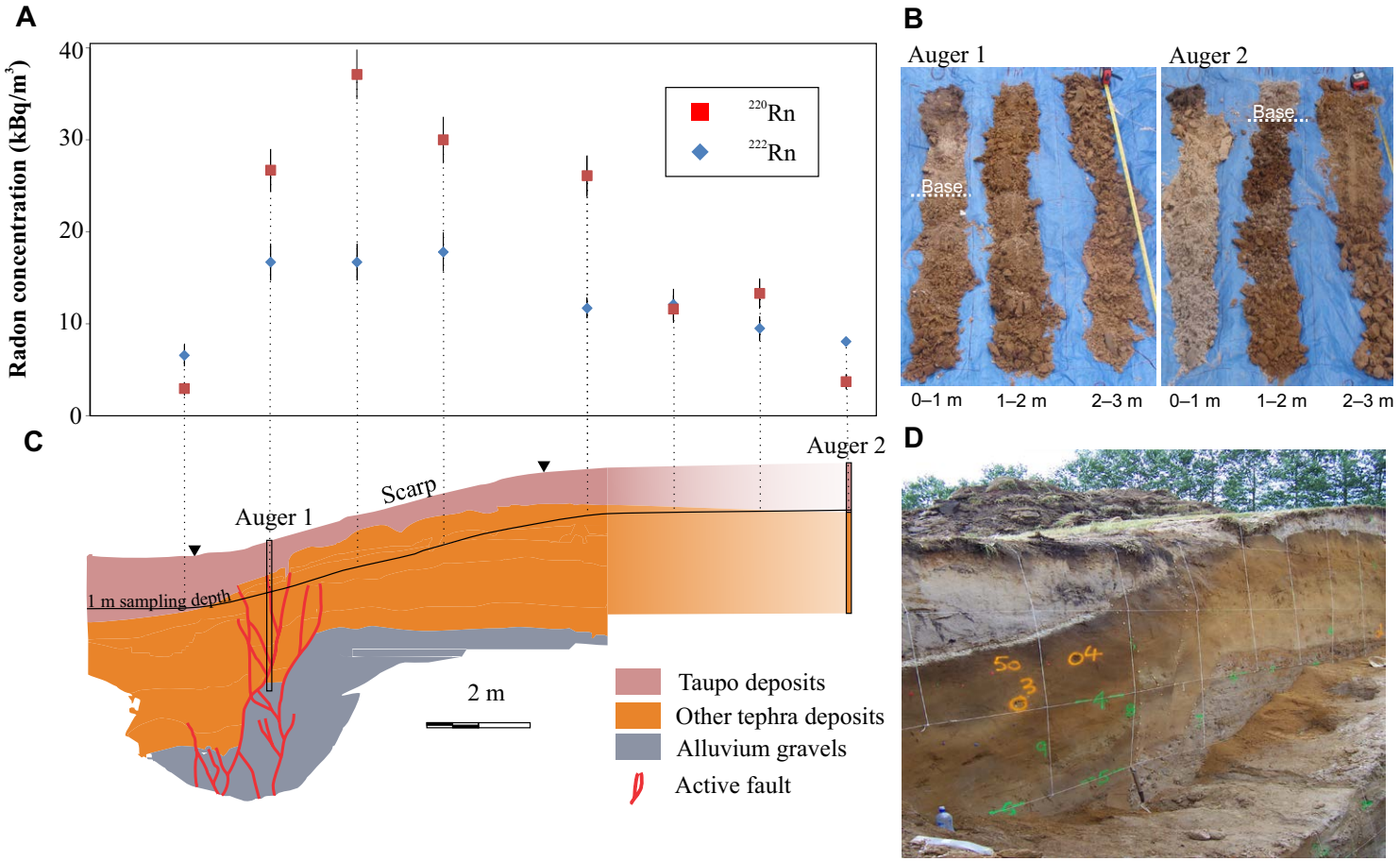

Figure 2. (A) Closely spaced soil gas radon concentration measurements across a scarp in the Maleme fault zone. Red squares indicate ^{220}Rn; blue diamonds indicate ^{222}Rn. See Figure 4 for the location of the profile. (B) Photograph of auger samples from two selected locations. The base of the Taupo deposits is highlighted in white in each auger sample. Note the color of the soil at 1 m depth, where the soil gas survey was collected. (C). Geological cross section of a trench across a scarp ~300 m east of A. Geology reproduced from McClymont et al. (2009). The grid string in photograph is 1 m square; a line is added to indicate hypothetical 1 m depth of soil gas sampling. Note the varying thickness of the gray Taupo ignimbrite deposits across the scarp. (D). Photograph of C.

fault is ~30 km long, strikes 040°–050°, and exposes a series of >100-m-thick ignimbrite units along the Paeroa Range (Keall, 1988; Villamor and Berryman, 2001; Downs et al., 2014). The vertical displacement of the ca. 350 ka Whakamaru Group ignimbrites is 550 m near Te Kopia, 10 km southwest of the study site, with an average displacement rate since their emplacement of ~1.5 mm/yr (Villamor and Berryman, 2001). Given its length, observed displacement, and displacement rate, the Paeroa fault probably cuts the entire brittle crust and extends to a depth of at least 8 km (Bibby et al., 1995; Nicol et al., 2010). In the region of study the Paeroa fault comprises two strands: the main Paeroa fault, with a scarp of ~200 m height, and a shorter strand in the hanging wall of the main trace having a scarp height of as much as ~20 m referred to as the Te Waro fault (Glover et al., 1992) (Fig. 3). Radon measurements have been collected along and across both strands of the Paeroa fault. Few data are currently available to locate the primary slip surfaces beneath these scarps; however, by analogy to Taupo rift trenching elsewhere (Villamor and Berryman, 2001; Berryman et al., 2008; Canora-Catalán et al., 2008; McClymont et al., 2009; Nicol et al., 2010) and published data on fault zone architecture (e.g., Childs et al., 2009), the geometries of these fault zones are expected to be highly variable. The Te Waro fault, as part of the Paeroa fault zone, probably intersects the main slip surface at depth. The maximum width of the Paeroa fault zone is probably greater than the Maleme faults, and fault-related fracturing of the ignimbrites is likely to have locally elevated permeability within the fault zones.

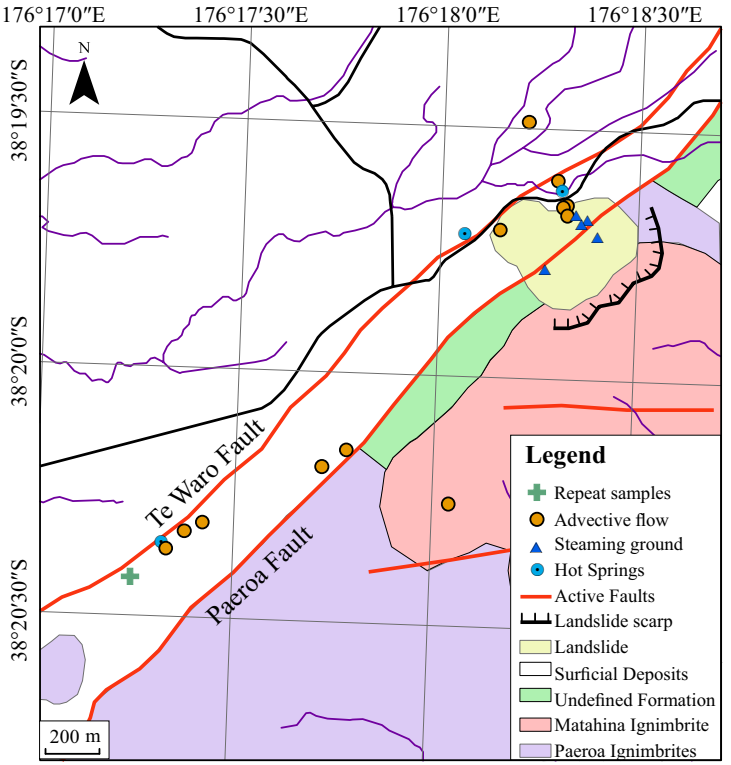

Figure 3. Geological map of the Waikite Valley area (after Grindley et al., 1994; Downs et al., 2014). The points in orange have a higher ^{222}Rn than can be accounted for by diffusion modeling (see discussion in text). The green cross indicates location of repeat samples. Active fault traces from Leonard et al. (2010).

The Paeroa fault is notable in that it is spatially associated with geothermal activity (e.g., hot springs, fumaroles, and hydrothermal deposits) at three locations along its strike (at Waikite, Te Kopia, and Orakei Korako) (Glover et al., 1992; Risk et al., 1994) (Fig. 1). The geothermal activity provides evidence of locally elevated permeability and vertical advective flow along the fault zone. The Waikite Spring is located near the base of the Paeroa scarp at the northern end of the field area, while Te Waro Spring further to the southwest flows from the base of the Te Waro scarp (Fig. 3). The Waikite Spring is a 98 °C boiling bicarbonate spring that flows at a rate of ~40 l/s (Glover et al., 1992). The bicarbonate content of the Waikite Spring, although heavily diluted compared to other New Zealand bicarbonate geothermal waters, suggests a distal source, most likely the Waiotapu geothermal field (Glover et al., 1992; Risk et al., 1994). Upslope of the main Waikite Spring within hummocky terrane of a landslide deposit, further geothermal activity is indicated by areas of steaming ground, sites of dead vegetation, hot (>30 °C) clay-rich soil and hydrothermal alteration. Te Waro scarp springs are significantly cooler than the Waikite Valley spring, reaching the ground surface at ~35 °C and forming a major tributary to the Te Waro stream (Glover et al., 1992). A number of radon samples were taken proximal to the Te Waro scarp springs and areas of steaming ground upslope of the Waikite Valley spring; the results of these samples are discussed in the following.

DATA COLLECTION AND METHODS

Radon in soil gas outside the geothermal areas was sampled at 1 m depth using a steel soil probe attached to a Durridge RAD7 radon detector. The sample depth was selected to mitigate variations in soil gas compositions due to atmospheric conditions (Clements and Wilkening, 1974; Malczewski and Zaba, 2007). In order to mitigate possible changes in radon concentration arising from rainfall, sampling of radon soil gas immediately after rainfall was avoided. To test the temporal and spatial reproducibility of radon results, 2 sites 2 m apart near the Te Waro scarp (Waikite Valley; Fig. 3) were sampled 7 times over a period of 3 weeks.

We collected 28 soil radon samples at Rehi Road in 2 transects trending normal to fault strike and separated by a distance of 150–200 m (Fig. 4). Each sample line crosses four fault traces; a radon measurement was collected from the top and bottom of each scarp. On the northernmost transect, eight samples were collected from a single scarp to analyze the detailed spatial

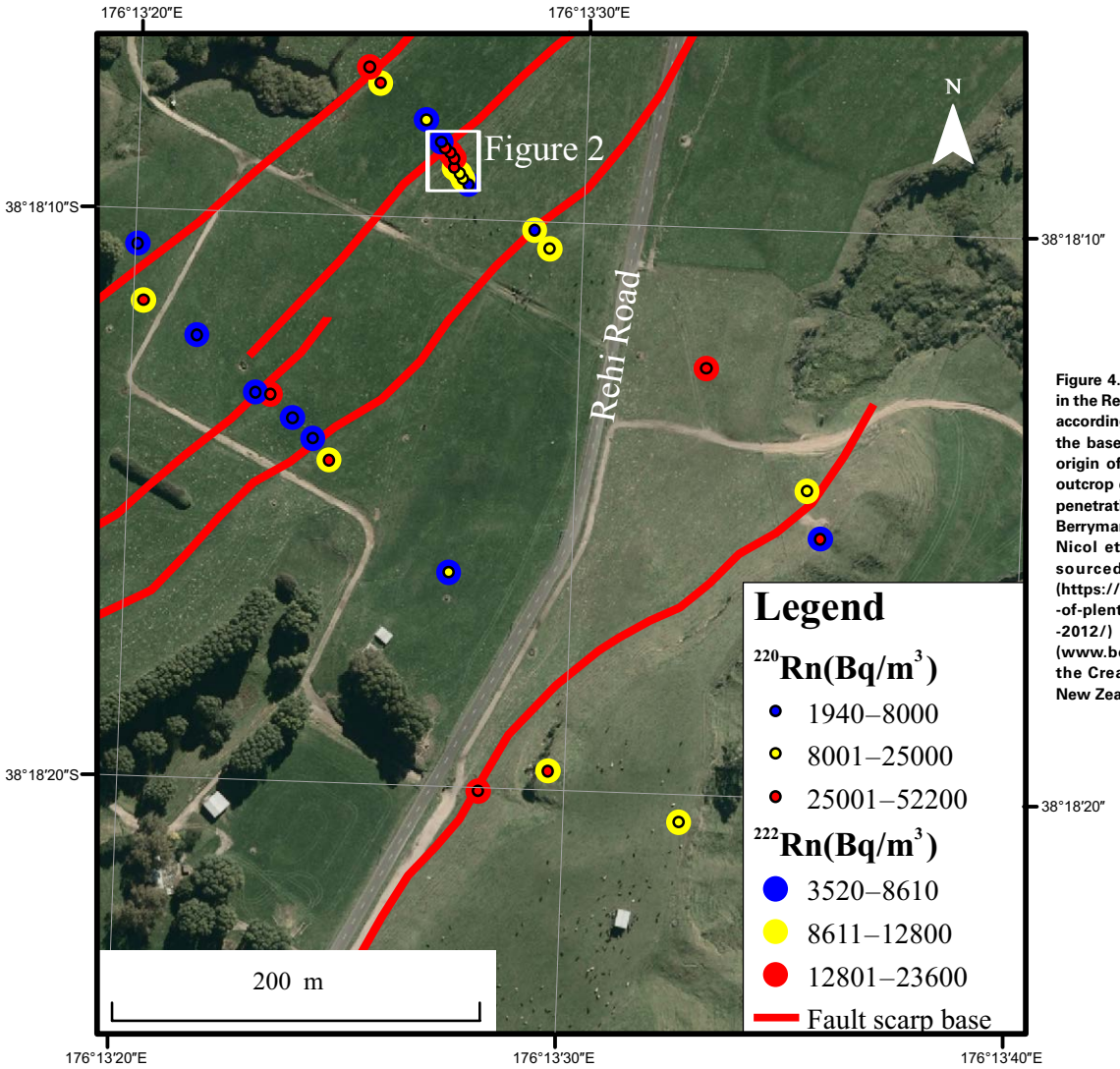

Figure 4. Map of soil gas survey locations in the Rehi Road area. The dots are colored according to Rn activity. Red lines mark the base of the scarps, with the tectonic origin of the scarps confirmed locally by outcrop exposures, trenching, and ground penetrating radar studies (Villamor and Berryman, 2001; McClymont et al., 2009; Nicol et al., 2010). Aerial photography sourced from the LINZ Data Service (https://data.linz.govt.nz/layer/1760-bay-of-plenty-025m-rural-aerial-photos-2011-2012/) and licensed by BOPLASS Ltd (www.boplass.govt.nz/) for reuse under the Creative Commons Attribution 3.0 New Zealand license.

variations in radon (see Figs. 2 and 4). Additional data were also collected halfway between the scarps to assess background radon and its variability in the absence of faulting.

In the Waikite Valley area sampling locations were split into two groups: (1) those measured near the scarps, and (2) background measurements. Samples were collected from the base and top of scarps (consistent with measurements at Rehi Road). Background measurements were collected from areas distal to the faults. For example, data were collected in the footwall of the main fault as much as 1 km from the top of the scarp. Samples were collected on grids with sample spacing of 25–50 m for a small area (~5×10^4 m^2) at the top of the Paeroa scarp and a larger area (~2×10^5 m^2) enclosing the Te Waro Spring (Fig. 5). Grid sampling was undertaken to quantify the spatial variability of radon

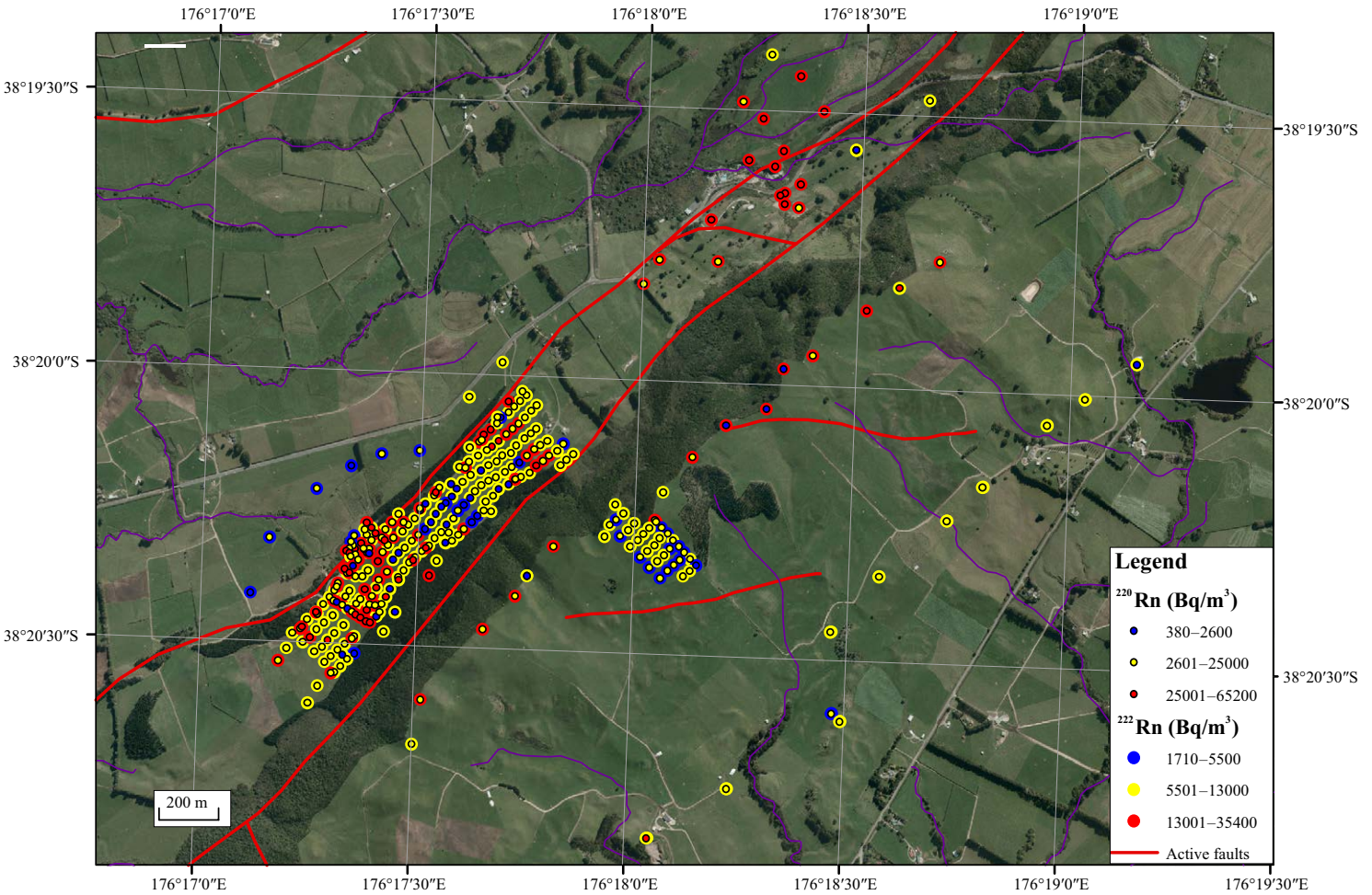

Figure 5. Map of soil gas survey locations in the Waikite Valley area. The dots are colored according to Rn activity. Aerial photograph sourced from the LINZ Data Service (https://data.linz.govt.nz/layer/1760-bay-of-plenty-025m-rural-aerial-photos-2011-2012/) and licensed by BOPLASS Ltd (www.boplass.govt.nz/) for reuse under the Creative Commons Attribution 3.0 New Zealand license. Active fault traces are from Leonard et al. (2010).

measurements along the scarp and around the Te Waro Spring. The scarps were too steep to be sampled, therefore no data are available for the scarps.

In addition to the measurements discussed here, steam was sampled from several small fumaroles and hot ground (>30 °C) located near the Waikite Spring (Fig. 3). The high temperature of the samples required the use of a cooling coil coupled with a smaller probe (30 cm). This setup differed from the one used for the soil gas survey, and therefore results are not directly comparable to the rest of the survey. However, all of the sampled hot ground sites were associated with extremely high ^{222}Rn concentrations and are briefly discussed with results from the non-geothermal samples in the next section.

Soil samples were retrieved by auger from depths of as much as 3 m at locations where soil gas was measured in both study areas (4 from Rehi Road and 13 from Waikite; see 2 examples in Fig. 2). Auger samples were collected to assess the near-surface stratigraphy, and to sample the radon

emanation potential of the soil at 1 m depth in a controlled environment. Soil samples retrieved from 1 m depth were inserted into a closed loop, and the Rn gas was measured within the loop. The closed loop method allowed for a relatively quick measurement of emission of ^{220}Rn isotope, as the sample containers reach secular equilibrium within minutes. However, a similar procedure would take ~16 days to reach secular equilibrium for ^{222}Rn. To collect ^{222}Rn emission data in a more practical time span, we estimated the parent concentration from the ^{222}Rn build-up over 24–48 h. This introduced a higher uncertainty for the ^{222}Rn measurements; however, the results are still significant and do not compromise the conclusions that can be drawn from the data.

RESULTS

The reproducibility tests show that temporal changes in ^{220}Rn concentrations at each sample point were generally uniform over time, with the measurement uncertainty being greater than the variability between measurements. A single ^{220}Rn measurement (27 January 2012, Site 2; see Fig. 6) does not fit this observation, because it was 25% lower than other values from the same site. As the concentration at the adjacent site was unchanged on 27 January 2012, it is possible that this low reading was due to experimental error. Measurements from these closely spaced samples in this study indicate that the ^{220}Rn for soil gas radon can be markedly spatially heterogeneous. The two sites tested for reproducibility are only ~2 m apart, yet the ^{220}Rn concentrations measured at the same time for each site differed by up to one order of magnitude (Fig. 6). However, ^{222}Rn values were more variable than ^{220}Rn over time, the maximum difference between the largest and smallest measurements during the course of the resampling program being ~25%.

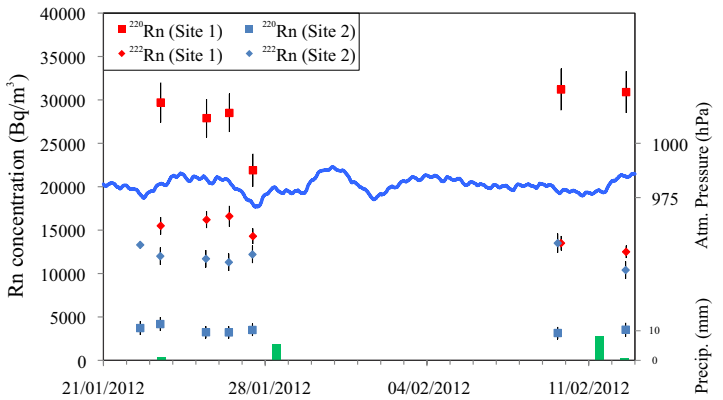

Figure 6. Repeated measurements over time for two sites (site 1 in blue, site 2 in red) located 2 m apart close to the Te Waro fault in the Waikite Valley area. Precipitation (Precip.; light green bars) and atmospheric (Atm.) pressure (blue line) from nearby Rotorua Airport (25 km north of the study area; data from the New Zealand National Institute of Water and Atmospheric Research National Climate Database, NIWA CliFlo; http://cliflo.niwa.co.nz/).

The ^{220}Rn and ^{222}Rn values are typically, but not exclusively, elevated proximal to scarps at the Rehi Road site (Fig. 4; Table 1); the tops of scarps have significantly higher ^{220}Rn measurements than at the base or between. In the closely spaced survey of 8 samples at Rehi Road, ^{220}Rn background concentrations vary between 2.96 and 13.3 Bq/m^3; scarp concentrations are as much as an order of magnitude higher, between 26.1 and 37.1 kBq/m^3 (Fig. 2). The ^{220}Rn gas profile along the detailed transect is asymmetric, with generally higher concentrations in the area of the scarp and hanging wall, and a rapid drop in concentration near the base of the scarp. The ^{222}Rn concentrations follow a similar trend to ^{220}Rn, being generally higher within the scarp than outside it (11.7–17.8 versus 6.57–12.1 kBq/m^3), although the difference in measurements between the scarp and background outside the scarp is less pronounced for ^{222}Rn than ^{220}Rn.

At Waikite Valley the soil gas survey results also indicate that ^{222}Rn concentrations are significantly higher closer to faults (Fig. 5; Table 1), with background values (>500 m from scarp) generally <13 kBq/m^3 and measurements near the scarps often greater than this value. The ^{220}Rn data appear to be slightly higher closer to the faults (the average is 16.1 kBq/m^3 near faults versus 14.5 kBq/m^3 for background data). However, the difference between the fault and background population is not statistically significant for ^{220}Rn (Table 1). The highest concentration of both radon isotopes (35.2 kBq/m^3 for ^{222}Rn and 65.2 kBq/m^3 for ^{220}Rn) occurs on the scarp near the Waikite geothermal area. This observation, along with the extreme values of both isotopes measured in steam emanating from the ground (~258 kBq/m^3 for ^{222}Rn and ~180 kBq/m^3 for ^{220}Rn), shows that the hot fluids in the geothermal system carry a significant amount of radium, which is common for bicarbonate springs (Wollenberg, 1974; Leonard and Janzer, 1977). The data distributions are log-normal for both radon isotopes over a significant range of concentrations (Fig. 7), showing that the populations are the products of multiple normally distributed independent variables (Limpert et al., 2001). The ^{220}Rn data set shows a clear bimodal distribution, with one log-normal population below 2.6 kBq/m^3, a second above

TABLE 1. MEANS OF DATA SETS AT REHI ROAD AND WAIKITE

	Rehi Road		
	Away from scarp	Top of scarp	Base of scarp
^{220}R	11.8 (7)	**29.4 (8)**	13.8 (8)
^{222}R	8.5 (7)	11.5 (8)	11.8 (8)
	Waikite		
	Near fault		Background (<500 m)
^{220}R	16.1 (299)		14.5 (11)
^{222}R	**11.3 (299)**		8.6 (11)

Notes: Number of samples in parentheses. Numbers in bold are data that are significantly higher (based on t-tests) than other populations in the same row.

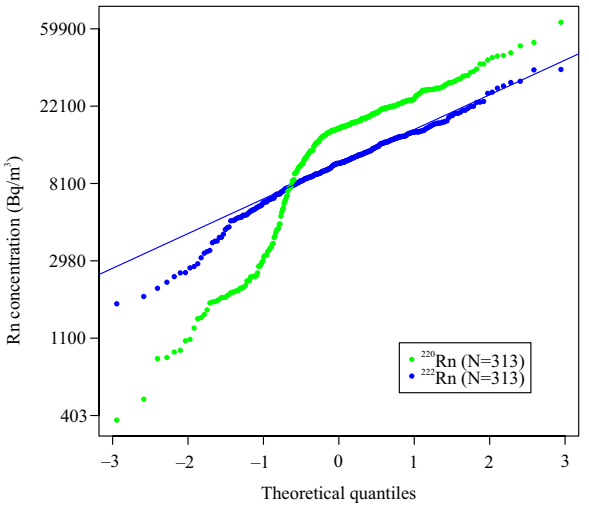

Figure 7. Waikite soil gas radon concentration quantile-quantile plot. The line represents the distribution of a log-normal population with the same mean and standard deviation as the ^{222}Rn population.

15 kBq/m³, and a mixing population between these values, whereas the ^{222}Rn concentration population seems to be unimodal.

Subsurface soil samples confirm the importance of soil type for radon concentrations. The stratigraphy to depths of as much as 3 m is mostly composed of fine-grained volcanic ash (tephra or ignimbrite deposits), with variable pumice clast content (≤2 cm in diameter). It is also possible that paleosol layers were intersected, such as identified at Rehi Road by others (Villamor and Berryman, 2001; McClymont et al., 2009; Nicol et al., 2010). Weathering of the deposits is highly variable; however, most auger holes encounter a sharp change at variable depth to a reddish-brown coloration due to oxidation or the presence of paleosols. This transition most likely represents the transition from the Taupo ignimbrite to older and more weathered tephras and paleosols. The water table was reached in one of the auger holes, at ~2.8 m, below which the degree of oxidation decreases. The auger hole results from the 13 samples recorded at Waikite Valley show a clear relationship between the color of the soil at 1 m depth and radon concentration recorded by the soil probe (e.g., Fig. 2). In circumstances where the soil is light gray and predominantly comprises volcanic tephra with little organic carbon, the ^{220}Rn values are relatively low (<~10 kBq/m³). By contrast, where the soil is light to dark brown, comprising a mix of oxidized tephras and possibly some organic carbon formed during paleosol development, the radon concentration is relatively high (>10 kBq/m³). These correlations between soil type and radon concentrations appear stronger for ^{220}Rn than ^{222}Rn and indicate that near-surface stratigraphy plays a key role in radon production of soil gas.

Laboratory measurements were taken from the auger samples in order to record production of radon in the soil gas. The radon emission results show a good correlation between ^{220}Rn collected in the field and laboratory (R^2 = 0.90, p value = 3 × 10^{-6}; Fig. 8A). By contrast, there is no significant linear relationship between the emission of ^{222}Rn measured in the laboratory and in the field for the same sample (R^2 = 0.17, p value = 0.17; Fig. 8B).

DISCUSSION

The method we used was repeatable for the ^{220}Rn isotopes as measurements are within the uncertainty; however, the ^{222}Rn isotope variability over time is much greater than the associated uncertainty (as great as 25% com-

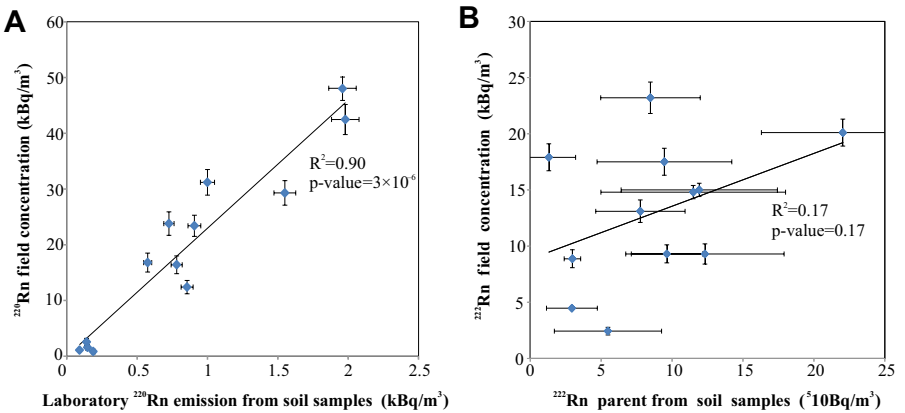

Figure 8. Field measurements compared to the laboratory emission results. (A) For ^{220}Rn. (B) For ^{222}Rn. Equation and R^2 for line of best fit are indicated on graph.

pared to a 10% uncertainty; Fig. 6). Several time-dependent factors could explain the ~25% variability over time of the ^{222}Rn, such as temperature, soil humidity, and/or soil gas CO_2 content. All of these factors change over time due to climatic effects (e.g., atmospheric pressure and precipitation) or bacterial processes. An increase in soil temperature can cause an increase in radon soil activity, most likely by release of adsorbed radon gas (Shefsky et al., 1993; Iskandar et al., 2004). While variation in soil humidity content can also affect the results, an increase in relative humidity tends to reduce the emanation of ^{220}Rn more readily than ^{222}Rn (Huxol et al., 2012). It is also possible that CO_2 concentration affected the RAD7 instrument (Tuccimei and Soligo, 2008), but this will likely have a greater influence on ^{220}Rn than ^{222}Rn isotopes (Lane-Smith and Sims, 2013) and cannot be called upon to account for the fluctuations in ^{222}Rn alone. Further inspection of Figure 6 does not reveal a clear correlation between ^{222}Rn concentrations and atmospheric pressure. The lowest ^{222}Rn values for both sites were taken on 12 February 2012, following a significant precipitation event; although this could indicate a correlation between soil humidity and ^{222}Rn, the fact that ^{220}Rn does not change seems to preclude this. It is possible that rainfall could be modifying soil permeability, affecting advective or diffusive processes of the longer half-life isotope, leaving the other isotope unchanged. Collectively, our sensitivity tests indicate that soil radon measurements provide information about geological processes (rather than climatic changes, for example) and support their use in this study.

Determining the cause or causes of a given radon anomaly near a fault is a complex undertaking, and involves the evaluation of a variety of site-specific conditions, including soil composition, soil permeability, presence or absence of potential carrier gases, and gas diffusion. The last two conditions are complicated by the radioactive characteristic of radon gas (^{222}Rn has a half-life of 3.82 days and ^{220}Rn has a half-life of 55.6 s), which limits its migration distance. For example, the diffusion length of ^{220}Rn is 20–31 mm, compared to 1600–2400 mm for ^{222}Rn (using diffusion coefficients of $D_{eff} = 5 \times 10^{-6}$ and 12×10^{-6} m^2/s, respectively; Tanner, 1978; Huxol et al., 2012). Even when assisted by a carrier gas in a relatively permeable saturated media, ^{220}Rn flowing at a velocity of centimeters per second (by bubble ascent; see Etiope, 2002) would only travel 80 cm before decaying to 1/*e* of its original concentration. However, if ^{222}Rn were carried by gas at velocities of 0.1–1 cm/s, it could travel distances of 500 m to 4 km before decaying to 1/*e* of the original concentration.

The difference in migration distance achieved by each isotope provides key information about the processes that result in their concentration proximal to faults. Because the ^{220}Rn nuclide is unlikely to travel distances >1 m (unless a high-velocity gas flow exists, such as might occur at a steam fumarole), it provides a powerful tool for measuring radon gas production within soil. In contrast, the ^{222}Rn nuclide could emanate from the soil or from deeper sources that, in some cases, may be kilometers below the ground surface. In circumstances where the concentrations of each isotope covary, it is more likely that an anomaly is due to an increase in the production of radon gases in the soil, rather than radon gases traveling by either diffusion or advection from a deeper source. Therefore, by comparing radon anomalies for each isotope, the local variation in soil radon emanation and flow of a radon-rich gas from depth can be distinguished.

The good correlation between laboratory and field measurement of ^{220}Rn (Fig. 8A), the correlation between soil color and ^{220}Rn concentration, the marked spatial heterogeneity of ^{220}Rn, and the bimodal distribution of ^{220}Rn are all consistent with the hypothesis that ^{220}Rn data measured in the field are the result of ^{220}Rn emission from the soil in which the gas sample was taken, and reflect the short half-life of the isotope. The short half-life impedes the diffusion or advection of the ^{220}Rn gas over long distances (~0.02 m or 0.8 m respectively), and therefore the concentration measured reflects the emission from the soil.

However, the lack of a significant linear correlation for ^{222}Rn between field and laboratory measurements (Fig. 8B), the low spatial variability of ^{222}Rn concentration (Fig. 6), and the single mode of distribution all clearly show that soil emanation is not the main process affecting the soil gas concentration of this isotope; and gas transport through soil is likely to be a cause of these results. Despite this last observation, linear regression models between the two isotopes at both the Waikite and the Rehi Road areas show significant positive correlations between ^{220}Rn and ^{222}Rn isotopes with a linear dependence between the two isotopes (Table 2; Fig. 9), with a relatively low R^2 value (0.44 and 0.54). Hence ^{222}Rn concentrations are systematically higher when the ^{220}Rn is elevated, albeit with some variability. This positive correlation suggests that a significant portion of ^{222}Rn measured in soil gas is derived from the soil. The positive correlation also allows us to confidently suggest that the ^{222}Rn anomaly observed in Figure 2 is mainly due to an increase in soil emanation of Rn gas.

The importance of near-surface stratigraphy for radon production in soil gas is further examined by comparing field measurements of the same material to those made in laboratory conditions (Fig. 10). The soil emission (laboratory) data of both isotopes are plotted against each other (Fig. 10B) and compared with the same plot for in situ soil gas measurements taken in the field before the samples were extracted (Fig. 10A; see Table 3 for a comparison summary). The linear-regression model for the field data in Figure 10A is similar to the overall Waikite data set (cf. Figs. 9 and 10A), with a positive slope, y-intercept, and significant linear correlation. This similarity suggests that conclusions drawn from comparison of the field and laboratory data may be applicable to the wider data set. However, unlike the field data set, the laboratory data have an intercept that is not significantly different from zero (3.84 ± 3.94; see Table 3). Even though the R^2 value is relatively low (R^2 = 0.49; Table 3), a

TABLE 2. LINEAR REGRESSION MODEL FOR ^{220}Rn VERSUS ^{222}Rn FOR EACH OF THE THREE SITES

	Waikite near fault	Waikite background	Rehi Road
Intercept	5738 ± 855	7452 ± 2379	6136 ± 2294
Slope	0.352 ± 0.044	0.082 ± 0.145	0.268 ± 0.096
R^2	0.44	0.023	0.54
Slope p value	$<2.2 \times 10^{-6}$	0.295	8.5×10^{-6}

Note: The ± value is 1.96× the standard error.

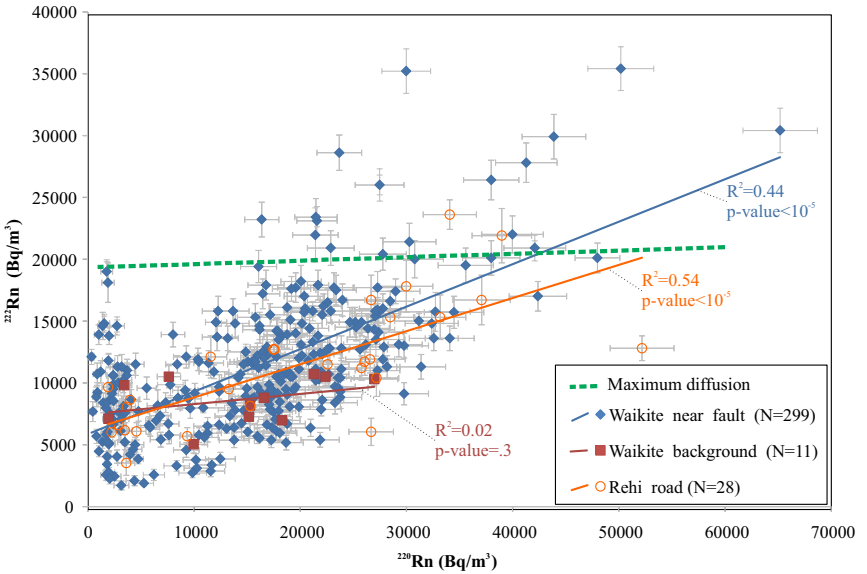

Figure 9. ^{220}Rn versus ^{222}Rn plot for all data from Waikite Valley and Rehi Road. The solid lines are the linear regression models for each data set (Table 2), colored the same as symbol color. The green dashed line represents the maximum concentration of ^{222}Rn achievable by small-scale diffusion (see discussion in text).

notable majority of the laboratory data plot on, or near to, a linear trend (see dashed line in Fig. 10B) with an intercept near the origin. The linear relationship of the regression models and the constancy of the slope of these models across different areas (Fig. 9; Table 2) indicate that, with the exception of the outliers, the radium parent ratio is in a majority of cases uniform (i.e., ^{224}Ra to ^{226}Ra ratio), and that the radon emanation coefficient varies between soil samples. This also reveals that the process affecting the ^{222}Rn isotope does not occur in the laboratory setting, consistent with the soil gas transport suggestion.

Therefore, we propose that the ^{222}Rn gas migrates over significant distances through the soil (>0.2 m) due to its longer half-life (~4 days compared to 55 s for ^{220}Rn). The concentration of gas produced locally is depleted or augmented by gas diffusion, and/or modified by advection of gas with a different ^{222}Rn concentration. Migration of ^{222}Rn is consistent with the observation that its concentration can vary significantly over time, unlike the ^{220}Rn concentration (Fig. 6). The ^{222}Rn gas would be expected to migrate from sites that have a high ^{220}Rn concentration to a low ^{220}Rn concentration. The positive intercept in

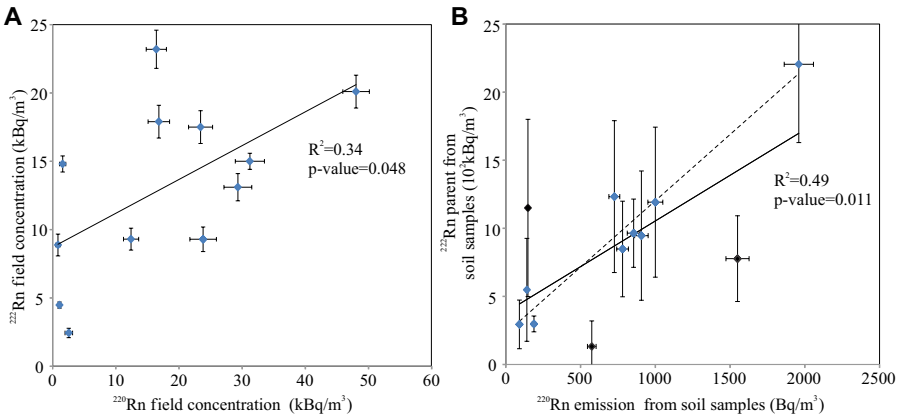

Figure 10. (A) Field radon concentration. (B) Laboratory soil emission results. The solid lines are the linear regression models (see Table 3). The dashed line is the linear regression line for the points excluding the three outliers, in black (see text).

TABLE 3. LINEAR REGRESSION MODELS FOR FIELD AND LABORATORY DATA

	Field data	Lab data
Intercept	8.71 ± 4.70	3.84 ± 3.94
Slope	0.24 ± 0.21	$6.71 \times 10^{-3} \pm 4.26 \times 10^{-3}$
R^2	0.34	0.488
p value	0.048	0.011

Note: ± is 1.96× the standard error.

the ^{220}Rn versus ^{222}Rn graphs suggests that there is higher ^{222}Rn than expected at low emanation potential sites. It is possible that these higher values were caused by (1) the diffusion of ^{222}Rn from nearby presence of soils with a higher emanation potential, (2) the advective flow of a gas with a ^{222}Rn concentration higher than background values, and/or (3) soils that have a different radon-parent ratio compared to the majority of the soils.

The question of whether the ^{222}Rn isotope is migrating by diffusion or advective flow of gases is further considered by analyzing the relative concentration of the radon isotopes and comparing their flow behavior to that expected for diffusion alone. Diffusion would cause ^{222}Rn gas produced in the soil to migrate from sites of higher concentration to sites of lower concentration. When ^{222}Rn gas diffuses from high to low emanation soils, the ^{222}Rn concentration measured at low emanation potential sites would be higher than ^{222}Rn production in the soil at these sites. The excess of ^{222}Rn created by diffusion of a radioactive isotope depends mostly on the distance between the sample site of the higher emanating soil, the magnitude of the production in both the proximal higher emanating soil and the local production, and the decay rate of the isotope. The diffusion profile for ^{222}Rn gas from ^{222}Rn producing soil has been modeled using the one-dimensional diffusion equation presented in Appendix 1. The highest concentration of ^{222}Rn produced by soil in the study areas, based on the highest ^{220}Rn measurement (65200 Bq/m^3) in these areas and multiplied by the potential parent ratio (0.352), gives a value of 23000 Bq/m^3. The extreme diffusion case, which would produce the highest excess ^{222}Rn for a given soil sample, is where ^{222}Rn was produced at 1.2 m depth at the highest rate measured in our field area (we estimate that our soil gas measurements sample a spherical volume of 20 cm, which is why we chose the 1.2 m, i.e., 0.2 m below the horizon sampled in soil gas measurements). The initial concentration is set to 23000 Bq/m^3 at 1.2 m, and the expected ^{222}Rn concentration at the measured depth, 1 m, is modeled based on the emanation potential of the soil (i.e., the ^{220}Rn concentration). Any ^{222}Rn concentrations above the model values could not be achieved by diffusion and prove that (1) a variation in the parent ratio and/or (2) input of ^{222}Rn by advection are processes that must be occurring at Waikite. The highest possible ^{222}Rn concentration for diffusion is plotted against ^{220}Rn, in other words, the emanation potential of the soil (dashed line in Fig. 9B). This plot shows that all but 12 points at Waikite (i.e., ~4% of the total) can potentially be explained by diffusion of ^{222}Rn gas within the soil using a single emanation ratio. The remaining anomalously high values from Waikite must be explained by the ^{222}Rn parent being more enriched than the ^{220}Rn parent and/or by the input of ^{222}Rn through advective flow of a radon-rich gas, and it is likely that other data points below this threshold are also affected by these processes.

High ^{222}Rn anomalies can in most cases be explained by local diffusion of Rn gas produced in the soil. Soil radon emanation power, or the radon emanation coefficient, is a function of the grain size of the soil (Tanner, 1978), the soil humidity (Huxol et al., 2012), and the location of the parent nuclide on or within the grain (i.e., in the grain or on the grain as a surface coating; Semkow and Parekh, 1990). The ^{220}Rn emanation could be related to clay minerals formed during soil production, which develop due to breakdown of humus, bioturbation of near-surface (< 0.5 m) sediments, and/or leaching of clay from higher permeable horizons (Easterbrook, 1999). It is also possible that relatively high radon was produced by a fluctuating water table, which causes oxidation and intense weathering (Taylor and Eggleton, 2001) and might reduce the grain size of minerals, increasing the relative surface area and the radon emanation. Whatever the precise mechanism that results in elevated radon emanation, our results indicate that the greatest values of radon occur in darker soils that occur below the ca. A.D. 1800 Taupo deposits (Fig. 2; Villamor and Berryman, 2001; McClymont et al., 2009; Nicol et al., 2010). Trenching of active faults in the Taupo rift indicates that the relative thickness of paleosol layers in the near-surface stratigraphy (<4 m) is often greatest on scarps, while the Taupo tephra interval can exceed 1 m in thickness in the immediate hanging walls of faults (Fig. 2; Villamor and Berryman, 2001; McClymont et al., 2009; Nicol et al., 2010). These bed geometries, which may partly reflect scarp erosion and associated amalgamation of paleosols, suggest that radon measurements on the scarps at 1 m depth are more likely than off-scarp sites to sample darker layers that emit more radon.

The locations of the soil samples that cannot be explained by diffusion are plotted in Figure 3. More than half of these points (7 of 12) plot within 100 m of known geothermal hot springs or fumaroles. These geothermal features are manifestations of advectively flowing fluids, and the observed ^{222}Rn could be affected by the flow of nearby fluids. The anomalies shown in Figure 3 may document the spatial distribution of permeable pathways within fault zones. The Waikite Valley hot springs together with the Te Kopia and the Orakei Korako geothermal fields are located on the Paeroa fault (see Fig. 1). Given the size of the fault (~28 km long and maximum throw of ~1100 m), it probably extends to the base of the continental crust (e.g., at 15–20 km depth; Stern et al., 2010) and intersects the fluid convective system in the rift. The coincidence of the fault and the geothermal areas is consistent with the fault being a conduit for the upward movement of hot geothermal fluids (e.g., Rowland and Sibson, 2004). At the Orakei Korako geothermal field, there is also evidence that low-permeability fault rock locally provides barriers to water flow and compartmentalizes the near-surface hydrology, as mapped normal faults produce a series of sinter-covered terraces that host perched boiling springs emanating from the bases of 5–10-m-high scarps (Lloyd, 1972). Given that the exact location of the fault slip surface could be within the scarp and not at the base of

the scarp, it is possible that this Rn survey missed some anomalously high Rn areas on the scarp if Rn-rich gas was coming up the fault.

Migration of a carrier gas can induce the flow of ^{222}Rn by advection over distances of kilometers. A flux of radon rich gas from depth, which is significantly different than background values, is required in order to use radon surveys as a tool for mapping faults or fluctuations in fluid flow within fault zones. The results shown in Figure 3 suggest that zones of high fluid flow along the Paeroa fault are restricted to specific locations, instead of the fault providing a continuous permeable pathway along its strike. Channelized flow of fluids along faults is a phenomenon that has been observed elsewhere in the Taupo rift (Seebeck et al., 2014).

CONCLUSIONS

The ^{222}Rn anomalies that have been recorded along scarps associated with faults in the Taupo rift support the results of previous studies (Tanner, 1978; Whitehead, 1984; King et al., 1996; Ciotoli et al., 1999; Al-Tamimi and Abumurad, 2001; Atallah et al., 2001; Ioannides, 2003; Burton et al., 2004; Font et al., 2008; Katsanou et al., 2010). Elevated radon gas concentrations close to scarps could be due to a number of processes, including flow of radon gas within fault zones and/or local variations in radon production arising from fault-related changes in near-surface stratigraphy. Field and laboratory observations support the hypothesis that ^{220}Rn field measurements are related to the local production of ^{220}Rn gas within the soil sample. The ^{222}Rn measurements can be partially attributed to local production; however, it is clear that the movement of the longer lived isotope is affected by other processes.

The results of this study show some clear evidence of advective flow of ^{222}Rn occurring at discrete, spatially restricted locations along the Paeroa fault. Most of these locations are associated with advectively flowing geothermal areas such as hot springs and fumaroles. Other radon anomalies around faults, which could also be caused by advection, are difficult to distinguish from anomalies that are caused by an increase in the radon emanation potential of soils.

An important outcome of this research is that ^{222}Rn soil gas concentration cannot be related to the emanation potential of the soil due to the potential diffusion of radon gas. Therefore, it is not possible to use the lack of a correlation between ^{222}Rn and ^{226}Ra or uranium as evidence for advective flow of ^{222}Rn gas. The ^{222}Rn anomalies that are associated with advective flow near faults are restricted to small areas within zones of high flux. In some cases, it is clear that the increase of radon emanation of the soil causes ^{222}Rn anomalies that are spatially associated with faults. With this in mind, if a fault was buried by a young geological formation, such as a sedimentary or volcanic deposit, the radon anomalies associated with the fault are likely to be undetectable if the deposit is thicker than several meters. It is therefore unlikely that blind faults will be detectable using radon soil gas surveys if they are buried at significant depths (e.g., >2 m).

APPENDIX 1. DIFFUSION MODEL

The governing equation that is used to model the diffusion of a radioactive gas is:

$$\frac{d^2\theta}{d\xi^2} = \alpha\theta - \beta, \quad (1)$$

where ξ, the dimensionless distance, is a function of the distance from the base of the considered area (x, in m) and L, the distance from base to the surface, and is defined as:

$$\xi = x/L; \quad (2)$$

θ, the dimensionless concentration, is a function of concentration at x (C, in mg/kg) and the initial concentration at $x = 0$(C_0, in mg/kg), defined as:

$$\theta = C/C_0. \quad (3)$$

The dimensionless decay constant, α, is a function of the decay constant of L, and of the radon isotope λ (in s^{-1}) and the diffusivity of the species in air, D ($m^2\ s^{-1}$):

$$\alpha = \lambda L^2/D, \quad (4)$$

and β is the dimensionless production rate, which is a function of R the species production rate (in kg s^{-1} m^{-3}), ρ, the density of air, and L, D, and C_0:

$$\beta = RL^2/D\rho C_0. \quad (5)$$

By imposing the following boundary conditions:

$$\theta(\xi = 0) = 1; \quad (6)$$

$$\theta(\xi = 1) + \varepsilon\frac{d\theta}{d\xi}(\xi = 1) = 0. \quad (7)$$

Here, ε is a function of the mass transfer Biot number, which controls the rate at which the gas is escaping from the soil profile at $\xi = 1$.

We get the following solution:

$$\theta = \frac{\left(1+\varepsilon\sqrt{\alpha}\right)(\beta-\alpha)e^{\sqrt{\alpha}} + \beta}{\alpha\left[\sinh\left(\sqrt{\alpha}\right) + \varepsilon\sqrt{\alpha}\cosh\left(\sqrt{\alpha}\right)\right]}\sinh\left(\sqrt{\alpha}\xi\right) + \left(1-\frac{\beta}{\alpha}\right)e^{\sqrt{\alpha}\xi} + \frac{\beta}{\alpha}. \quad (8)$$

In order to model the highest possible concentration (θ) that could be achieved by diffusion, we consider the distance from 1.2 m depth (i.e., just below our measurement depth) to the surface (Table A1). At 1.2 m we consider C_0 to be the highest possible concentration achievable through production in soil, which we estimate by multiplying the highest ^{220}Rn concentration measured in the field (i.e. the highest soil radon emanation, 65.3 kBq/m^3) by the dominant parent ratio from the linear model at Waikite (0.337), which gives us a C_0 of 22.0 kBq/m^3 (or 9.35×10^{-8} mg/kg, if ρ = 1.225 kg/m^3).

TABLE A1. PARAMETER VALUES CHOSEN FOR DIFFUSION MODEL AND THEIR RESPECTIVE SENSITIVITY

Parameter	Value	Sensitivity
C_0	9.35×10^{-8}	high
L	1.2	medium
l	2.09×10^{-6}	high
D	1.2	low
r	1.225	low
h	2.04×10^{-4}	low
R	variable, depending on ^{220}Rn	low to high

Notes: The recharge rate was assumed to be a function of the ^{220}Rn emanation rate, and hence the radon soil emanation rate. In this situation, it is practical that radon concentration is measured in Bq/m^3, as this measures the number of radon nuclides decaying/cubic meter. We assume that the ^{220}Rn concentration that we measure is in secular equilibrium with the production rate, and that therefore the number of radon decay/second is equivalent to the number of radon being produced. In the case of the ^{222}Rn production rate, we use the dominant parent ratio in order to estimate the recharge from the ^{220}Rn decay rate.

ACKNOWLEDGMENTS

We acknowledge Jim Cole, Travis Horton, Chris Oze, Tom Powell, and Marie-Claude Hébert for feedback on the manuscript, Tom Garden, Cameron Asher, and Tom Powell for help with field work, Derek Lane-Smith for help with the RAD7 instrument, Kevin Finnerty for help in Waikite Valley, and Rens from Ngapouri Road for granting access to the paddocks. The author wishes to thank Mike Cheadle and one anonymous reviewer for their comments that substantially improved this manuscript. This research was funded by Mighty River Power through the Source to Surface Program.

REFERENCES CITED

Al-Tamimi, M.H., and Abumurad, K.M., 2001, Radon anomalies along faults in north of Jordan: Radiation Measurements, v. 34, p. 397–400, doi:10.1016/S1350-4487(01)00193-7.

Atallah, M.Y., Al-Bataina, B.A., and Mustafa, H., 2001, Radon emanation along the Dead Sea transform (rift) in Jordan: Environmental Geology, v. 40, p. 1440–1446, doi:10.1007/s002540100337.

Bégué, F., Gravley, D.M., Chambefort, I., Deering, C., and Kennedy, B., 2014, Magmatic volatile distribution as recorded by rhyolitic melt inclusions in the Taupo Volcanic Zone, New Zealand, *in* Zellmer, G.F., et al., eds., The Role of Volatiles in the Genesis, Evolution and Eruption of Arc Magmas: Geological Society of London Special Publication 410, p. 71–94, doi:10.1144/SP410.4.

Berryman, K., Villamor, P., Nairn, I., Van Dissen, R., Begg, J., and Lee, J., 2008, Late Quaternary surface rupture history of the Paeroa Fault, Taupo Rift, New Zealand: New Zealand Journal of Geology and Geophysics, v. 51, p. 135–158, doi:10.1080/00288300809509855.

Bibby, H.M., Caldwell, T.G., Davey, F., and Webb, T.H., 1995, Geophysical evidence on the structure of the Taupo Volcanic Zone and its hydrothermal circulation: Journal of Volcanology and Geothermal Research, v. 68, p. 29–58, doi:10.1016/0377-0273(95)00007-H.

Burton, M., Neri, M., and Condarelli, D., 2004, High spatial resolution radon measurements reveal hidden active faults on Mt. Etna: Geophysical Research Letters, v. 31, L07618, doi:10.1029/2003GL019181.

Canora-Catalán, C., Villamor, P., Berryman, K., Martínez-Díaz, J.J., and Raen, T., 2008, Rupture history of the Whirinaki fault, an active normal fault in the Taupo Rift, New Zealand: New Zealand Journal of Geology and Geophysics, v. 51, p. 277–293, doi:10.1080/00288300809509866.

Childs, C., Manzocchi, T., Walsh, J.J., Bonson, C.G., Nicol, A., and Schöpfer, M.P., 2009, A geometric model of fault zone and fault rock thickness variations: Journal of Structural Geology, v. 31, p. 117–127, doi:10.1016/j.jsg.2008.08.009.

Ciotoli, G., Etiope, G., Guerra, M., and Lombardi, S., 1999, The detection of concealed faults in the Ofanto Basin using the correlation between soil-gas fracture surveys: Tectonophysics, v. 301, p. 321–332, doi:10.1016/S0040-1951(98)00220-0.

Clements, W.E., and Wilkening, M.H., 1974, Atmospheric pressure effects on ^{222}Rn transport across the earth-air interface: Journal of Geophysical Research, v. 79, p. 5025–5029, doi:10.1029/JC079i033p05025.

Cole, J.W., 1990, Structural control and origin of volcanism in the Taupo volcanic zone, New Zealand: Bulletin of Volcanology, v. 52, p. 445–459, doi:10.1007/BF00268925.

Downs, D.T., Rowland, J.V., Wilson, C.J.N., Rosenberg, M.D., Leonard, G.S., and Calvert, A.T., 2014, Evolution of the intra-arc Taupo-Reporoa Basin within the Taupo Volcanic Zone of New Zealand: Geosphere, v. 10, p. 185–206, doi:10.1130/GES00965.1.

Easterbrook, D.J., 1999, Surface Processes and Landforms (second edition): Upper Saddle River, New Jersey, Prentice Hall, 546 p.

Etiope, G., 2002, Migration of carrier and trace gases in the geosphere: An overview: Physics of the Earth and Planetary Interiors, v. 129, p. 185–204, doi:10.1016/S0031-9201(01)00292-8.

Font, L., Baixeras, C., Moreno, V., and Bach, J., 2008, Soil radon levels across the Amer fault: Radiation Measurements, v. 43, p. S319–S323, doi:10.1016/j.radmeas.2008.04.072.

Glover, R., Klyen, L., and Crump, M., 1992, Spring chemistry of the Waikite-Paukohurea thermal area: Proceedings, 14th New Zealand Geothermal Workshop, p. 63–72.

Grindley, G., Mumme, T., and Kohn, B., 1994, Stratigraphy, paleomagnetism, geochronology and structure of silicic volcanic rocks, Waiotapu/Paeroa Range area, New Zealand: Geothermics, v. 23, p. 473–499, doi:10.1016/0375-6505(94)90014-0.

Holub, R.F., and Brady, B.T., 1981, The effect of stress on radon emanation from rock: Journal of Geophysical Research, v. 86, p. 1776–1784, doi:10.1029/JB086iB03p01776.

Huxol, S., Brennwald, M.S., Hoehn, E., and Kipfer, R., 2012, On the fate of ^{220}Rn in soil material in dependence of water content: Implications from field and laboratory experiments: Chemical Geology, v. 298–299, p. 116–122, doi:10.1016/j.chemgeo.2012.01.002.

Ioannides, K., 2003, Soil gas radon: A tool for exploring active fault zones: Applied Radiation and Isotopes, v. 59, p. 205–213, doi:10.1016/S0969-8043(03)00164-7.

Iskandar, D., Yamazawa, H., and Iida, T., 2004, Quantification of the dependency of radon emanation power on soil temperature: Applied Radiation and Isotopes, v. 60, p. 971–973, doi:10.1016/j.apradiso.2004.02.003.

Israel, H., and Bjornsson, S., 1967, Radon (Rn-222) and Thoron (Rn-220) in soil air over faults: Zeitschrift für Geophysik, v. 33, p. 48–64.

Katsanou, K., Stratikopoulos, K., Zagana, E., and Lambrakis, N., 2010, Radon changes along main faults in the broader Aigion region, NW Peloponnese: Bulletin of the Geological Society of Greece, v. 43, p. 1726–1736.

Keall, J.M., 1988, Volcanology and ignimbrite stratigraphy along the Paeroa Fault, Taupo Volcanic Zone [M.Sc. thesis]: Wellington, New Zealand, Victoria University, 118 p.

King, C.-Y., King, B.-S., Evans, W.C., and Zhang, W., 1996, Spatial radon anomalies on active faults in California: Applied Geochemistry, v. 11, p. 497–510, doi:10.1016/0883-2927(96)00003-0.

Koike, K., Yoshinaga, T., Suetsugu, K., Kashiwaya, K., and Asaue, H., 2015, Controls on radon emission from granite as evidenced by compression testing to failure: Geophysical Journal International, v. 203, p. 428–436, doi:10.1093/gji/ggv290.

Lane-Smith, D., and Sims, K.W.W., 2013, The effect of CO_2 on the measurement of ^{220}Rn and ^{222}Rn with instruments utilising electrostatic precipitation: Acta Geophysica. v. 61, p. 822–830, doi:10.2478/s11600-013-0107-3.

Leonard, G.S., Begg, J.G., and Wilson, C.J.N., 2010, Geology of the Rotorua area: Geological map 5: Lower Hutt, New Zealand, Geological & Nuclear Sciences Institute, scale 1:250,000, 99 p.

Leonard, R.B., and Janzer, V.J., 1977, Natural radioactivity in geothermal waters, Alhambra Hot Springs and nearby areas, Jefferson County, Montana: U.S. Geological Survey Journal of Research, v. 6, p. 529–540.

Limpert, E., Stahel, W.A., and Abbt, M., 2001, Log-normal distributions across the sciences: Keys and clues: Bioscience, v. 51, p. 341–352, doi:10.1641/0006-3568(2001)051[0341:LNDATS]2.0.CO;2.

Lloyd, E.F., 1972, Geology and hot springs of Orakeikorako, New Zealand: New Zealand Geological Survey Bulletin 85, 164 p.

Malczewski, D., and Zaba, J., 2007, ^{222}Rn and ^{220}Rn concentrations in soil gas of Karkonosze-Izera Block (Sudetes, Poland): Journal of Environmental Radioactivity, v. 92, p. 144–164, doi:10.1016/j.jenvrad.2006.11.001.

McClymont, A.F., Villamor, P., and Green, A.G., 2009, Fault displacement accumulation and slip rate variability within the Taupo Rift (New Zealand) based on trench and 3-D ground penetrating radar data: Tectonics, v. 28, TC4005, doi:10.1029/2008TC002334.

Mollo, S., Tuccimei, P., Heap, M.J., Vinciguerra, S., Soligo, M., Castelluccio, M., and Dingwell, D.B., 2011, Increase in radon emission due to rock failure: An experimental study: Geophysical Research Letters, v. 38, L14304, doi:10.1029/2011GL047962.

Nicol, A., Walsh, J.J., Villamor, P., Seebeck, H.C., and Berryman, K.R., 2010, Normal fault interactions, paleoearthquakes and growth in an active rift: Journal of Structural Geology, v. 32, p. 1101–1113, doi:10.1016/j.jsg.2010.06.018.

Risk, H., Caldwell, T., and Bibby, H., 1994, Deep resistivity surveys in the Waiotapu-Waikite-Reporoa region, New Zealand: Geothermics, v. 23, p. 423–443, doi:10.1016/0375-6505(94)90012-4.

Rowland, J.V., and Sibson, R.H., 2001, Extensional fault kinematics within the Taupo Volcanic Zone, New Zealand: Soft-linked segmentation of a continental rift system: New Zealand Journal of Geology and Geophysics, v. 44, p. 271–283, doi:10.1080/00288306.2001.9514938.

Rowland, J.V., and Sibson, R.H., 2004, Structural controls on hydrothermal flow in a segmented rift system, Taupo Volcanic Zone, New Zealand: Geofluids, v. 4, p. 259–283, doi:10.1111/j.1468-8123.2004.00091.x.

Seebeck, H.C., Nicol, A., Walsh, J.J., Childs, C., Beetham, R.D., and Pettinga, J., 2014, Fluid flow in fault zones from an active rift: Journal of Structural Geology v. 62, p .52–64, doi:10.1016/j.jsg.2014.01.008.

Semkow, T.M., and Parekh, P.P., 1990, The role of radium distribution and porosity in radon emanation from solids: Geophysical Research Letters, v. 17, p. 837–840, doi:10.1029/GL017i006p00837.

Shefsky, S.I., Rose, D., and Parsons, C.G., 1993, A study of radon adsorption on activated carbon as a function of temperature, *in* Proceedings, 1993 International Radon Conference: Fletcher, North Carolina, American Association of Radon Scientists and Technologists, p. 12–18.

Stern, T., Stratford, W., Seward, A., Henderson, M., Savage, M., Smith, E., Benson, A., Greve, S., and Salmon, S., 2010, Crust-mantle structure of the central North Island, New Zealand, based on seismological observations: Journal of Volcanology and Geothermal Research, v. 190, p. 58–74, doi:10.1016/j.jvolgeores.2009.11.017.

Stratford, W.R., and Stern, T.A., 2006, Crust and upper mantle structure of a continental backarc: Central North Island, New Zealand: Geophysical Journal International, v. 166, p. 469–484, doi:10.1111/j.1365-246X.2006.02967.x.

Tanner, A.B., 1964, Physical and chemical controls on distribution of radium-226 and radon-222 in ground water near Great Salt Lake, Utah, *in* Adams, J.A.S., and Lowder, W.M., eds., The Natural Radiation Environment: Chicago, University of Chicago Press, p. 253–276.

Tanner, A.B., 1978, Radon migration in the ground: A supplementary review: U.S. Geological Survey Open-File Report 78-1050, 61 p.

Taylor, G., and Eggleton, R.A., 2001, Regolith Geology and Geomorphology: Chichester, UK, John Wiley and Sons, 375 p.

Tuccimei, P., and Soligo, M., 2008, Correcting for CO_2 interference in soil radon flux measurements: Radiation Measurements, v. 43, p. 102–105, doi:10.1016/j.radmeas.2007.05.056.

Tuccimei, P., Mollo, S., Vinciguerra, S., Castelluccio, M., and Soligo, M., 2010, Radon and thoron emission from lithophysae-rich tuff under increasing deformation: An experimental study: Geophysical Research Letters, v. 37, L05305, doi:10.1029/2009GL042134.

Villamor, P., and Berryman, K.R., 2001, A late Quaternary extension rate in the Taupo Volcanic Zone, New Zealand, derived from fault slip data: New Zealand Journal of Geology and Geophysics, v. 44, p. 243–269, doi:10.1080/00288306.2001.9514937.

Vogler, G., 1960, Ursachen emanometrischer Anomalien: Zeitschrift für Geophysik, v. 26, p. 57–71.

Whitehead, N., 1984, Geothermal prospecting by ground radon measurements: Journal of Volcanology and Geothermal Research, v. 20, p. 213–229, doi:10.1016/0377-0273(84)90040-4.

Wilson, C.J.N., Houghton, B.F., McWilliams, M.O., Lanphere, M.A., Weaver, S.D., and Briggs, R.M., 1995, Volcanic and structural evolution of Taupo Volcanic Zone, New Zealand: A review: Journal of Volcanology and Geothermal Research, v. 68, p. 1–28, doi:10.1016/0377-0273(95)00006-G.

Wollenberg, H.A., 1974, Radioactivity of Nevada hot-spring systems: Geophysical Research Letters, v. 1, p. 359–362, doi:10.1029/GL001i008p00359.

Wright, I.C., 1992, Shallow structure and active tectonism of an offshore continental back-arc spreading system: The Taupo Volcanic Zone, New Zealand: Marine Geology, v. 103, p. 287–309, doi:10.1016/0025-3227(92)90021-9.

Zarroca, M., Linares, R., Bach, J., Roqué, C., Moreno, V., Font, L., and Baixeras, C., 2012, Integrated geophysics and soil gas profiles as a tool to characterize active faults: The Amer fault example (Pyrenees, NE Spain): Environmental Earth Sciences, v. 67, p. 889–910, doi:10.1007/s12665-012-1537-y.